ACS Photonics

Article

pubs.acs.org/journal/apchd5

Nanogap-Enhanced Terahertz Sensing of 1 nm Thick ($\lambda/10^6$) Dielectric Films

Hyeong-Ryeol Park,[†,‡] Xiaoshu Chen,[†,‡] Ngoc-Cuong Nguyen,[‡,§] Jaime Peraire,*[,§] and Sang-Hyun Oh*[,†]

[†]Department of Electrical and Computer Engineering, University of Minnesota, Minneapolis, Minnesota 55455, United States

[§]Department of Aeronautics and Astronautics, Massachusetts Institute of Technology, Cambridge, Massachusetts 02139, United States

Supporting Information

ABSTRACT: We experimentally show that terahertz (THz) waves confined in sub-10 nm metallic gaps can detect refractive index changes caused by only a 1 nm thick ($\sim\lambda/10^6$) dielectric overlayer. We use atomic layer lithography to fabricate a wafer-scale array of annular nanogaps. Using THz time-domain spectroscopy in conjunction with atomic layer deposition, we measure spectral shifts of a THz resonance peak with increasing Al_2O_3 film thickness in 1 nm intervals. Because of the enormous mismatch in length scales between THz waves and sub-10 nm gaps, conventional modeling techniques cannot readily be used to analyze our results. We employ an advanced finite-element-modeling (FEM) technique, Hybridizable Discontinuous Galerkin (HDG) scheme, for full three-dimensional modeling of the resonant transmission of THz waves through an annular gap that is 2 nm in width and 32 μm in diameter. Our multiscale 3D FEM technique and atomic layer lithography will enable a series of new investigations in THz nanophotonics that has not been possible before.

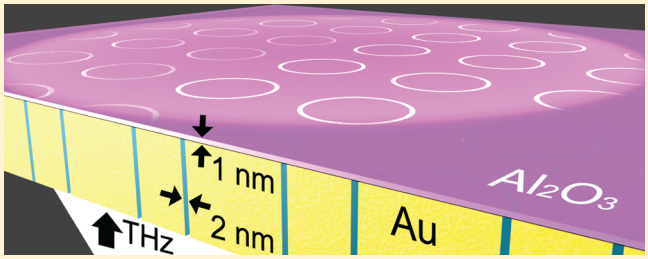

KEYWORDS: *nanogap, thin-film sensing, atomic layer deposition, atomic layer lithography, finite element modeling, Hybridizable Discontinuous Galerkin (HDG) method, terahertz nanophotonics*

Extraordinary optical transmission (EOT) through subwavelength apertures in a metal film, wherein the amount of optical transmission is higher than the amount of light incident on open areas, has been widely utilized for optical sensing and spectroscopy applications in the visible, infrared, and terahertz regimes.[1−5] While initial studies on the EOT effect focused on circular and rectangular apertures, annular apertures, or coaxial waveguides, in a metal film also exhibit the EOT effect and large field enhancements as the gap size shrinks.[6−8] Annular apertures also possess tunable ring resonances along the contour. For a fixed gap width, increasing the contour length of each loop can shift the resonance frequency from visible (for an annulus diameter on the order of ~100 nm)[7−9] to infrared (diameter of ~1 μm),[10] and THz[11,12] frequencies (diameter of 10 μm to ~1 mm). With simpler hole geometries, such broadband tuning while maintaining nanometer-sized aperture is not possible. The EOT effect in an annular aperture becomes even more dramatic in the THz frequency range (0.1 to 1.0 THz), where the optical properties of metals approach that of perfect electrical conductors. In this technologically important yet underexplored frequency regime,[13] the capability to confine and boost electric fields in deep subwavelength apertures can lead to novel applications in sensing,[14−17] optical modulation,[12,18] and THz fingerprinting of molecules.[19,20]

While THz waves have been utilized for sensing thin-film materials, there exists an intrinsic limitation to measure nanometer-thick film with millimeter-scale THz waves due to the extreme size mismatch and the lack of tight field confinement in the THz regime. Previous experiments based on THz time-domain spectroscopy (THz-TDS) reported a minimum detectable film thickness of several microns for common dielectric materials such as photoresist and polydimethylsiloxane (PDMS).[14,15,21] Even for materials that absorb THz radiation such as water and DNA, typically a layer thicker than a few hundred nanometers is required for unambiguous detection.[22−24] Compared with surface plasmon resonance (SPR) sensing in the visible regime,[25] which can readily detect spectral shifts due to 1 nm thick or even sub-nm thick dielectric films, the thin-film sensing capability of THz waves is poor because of the wavelength-to-film thickness mismatch. Various schemes, including waveguides,[23] slot antennas,[20] and metamaterials,[14,15,24] have been employed to enhance the interaction of THz waves with thin films, but the detection of refractive index changes due to nanometer thick dielectric films has not been possible.

Here we present a solution to overcome this challenge by squeezing a THz wave inside nanometer-wide annular gaps in a gold film and use its tightly localized near-fields for sensing 1 nm thick dielectric films. These annular gap devices are designed to sustain resonances at THz frequencies, and we measure the changes in resonance frequencies resulting from a sequential

Received: December 9, 2014
Published: February 4, 2015

DOI: 10.1021/ph500464j
ACS Photonics 2015, 2, 417−424

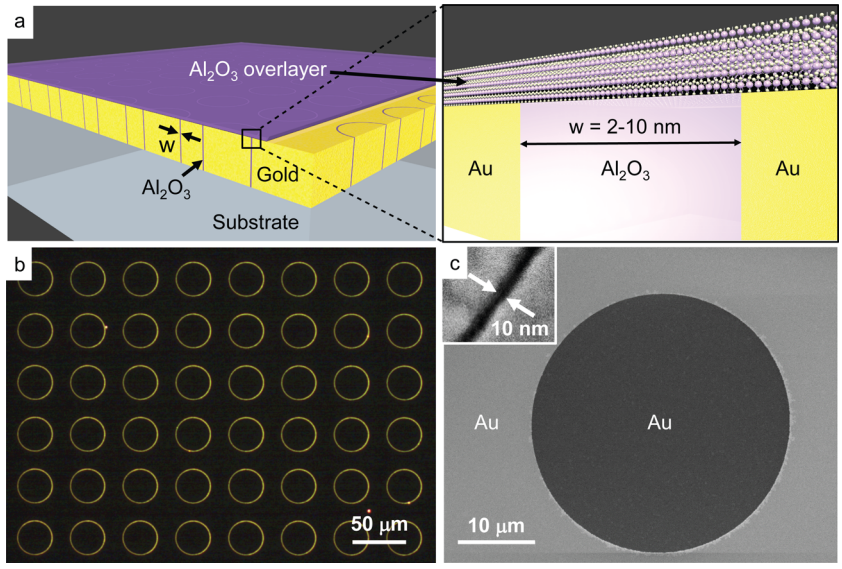

Figure 1. (a) Schematic diagram of an Al_2O_3 ultrathin layer on an annular gap array with a gap size of w (=2, 5, and 10 nm), a diameter of 32 μm, and a period of 50 μm in a 150 nm thick gold film on a glass substrate. (Inset) Enlarged illustration of the ALD-deposited Al_2O_3 overlayer on the nanogap, which is filled with Al_2O_3. (b) Top-view microscope image of the annular gaps with the gap size of 10 nm, the loop length of 100 μm, and the total image area of 0.3 mm × 0.4 mm. (c) Scanning electron micrograph (SEM) of an annular gap with a gap size of 10 nm and a diameter of 32 μm. (Inset) Enlarged SEM image of the same 10 nm gap formed along the contour of the annular aperture. The different colors for the inner and outer gold areas are caused by the presence of a Ti adhesion layer underneath the outer area.

atomic layer deposition (ALD) of only 1 nm thick Al_2O_3 overlayers on the annular gaps. For theoretical analysis of these results, we also address the extreme multiscale computational challenges, that is, full three-dimensional (3D) modeling of millimeter waves passing through nanometer-wide gaps using an advanced finite-element method (FEM) technique called Hybridizable Discontinuous Galerkin (HDG) scheme.

RESULTS AND DISCUSSION

Schematic illustrations (Figure 1a) show the device geometries used in this work. For the nanometer-scale localization of THz waves, we employ atomic-layer lithography[26,27] to create sub-10 nm gaps in gold films. The key strength of this patterning technique is that the critical dimension, that is, the gap width, is decoupled from the overall size of the pattern; thus it is possible to produce nanometer-wide gaps along loops that are even at the centimeter-scale.[28] In this work, a sub-10 nm gap in a metal film is extended to form a loop with a diameter of 32 μm, which is chosen to create strong annular loop resonances at THz frequencies. To increase the signal-to-noise ratio for detection, these annular nanogap loops were patterned into a wafer-scale array with a 50 μm periodicity (Figure 1b). Samples with gap sizes of 2, 5, and 10 nm were fabricated (Figure 1c).[27]

While the fabrication challenge of producing a dense array of sub-10 nm annular apertures is addressed via atomic layer lithography, accurate computational modeling of THz wave propagation inside the large loop of a sub-10 nm gap poses another significant challenge.[29] The enormous mismatch in length scales, up to 6 orders of magnitude between millimeter-scale wavelength and nanometer-scale gap size, is beyond the capabilities of currently available finite-difference time-domain (FDTD) or finite-element (FE) methods. To solve this problem, we develop and employ a sophisticated numerical algorithm, called Hybridizable Discontinuous Galerkin (HDG) method,[30] to calculate full 3D field distributions and transmission spectra for the whole structure in a fast and accurate manner.

Discontinuous Galerkin (DG) methods[31−34] have received considerable attention in computational electromagnetics[35] because they possess many attractive characteristics for solving Maxwell's equations in time and frequency domains. In particular, they are unstructured, locally conservative, high-order accurate, low dissipative and dispersive, and optimally convergent,[36] whereas FDTD methods generally lack of these desirable features. Despite these advantages, most current DG methods are computationally expensive due to the fact that they have duplicate degrees of freedom on the interior element faces.[37] This shortcoming of DG methods is the main motivation behind the development of the HDG method.[38−40] The HDG method not only retains the aforementioned advantages of DG methods, but also possesses additional crucial advantages that make it ideally suited for computational electromagnetics. First, the HDG method reduces the global unknowns to the tangential approximate trace of the electric field,[30] which has only two components without the duplication of degrees of freedom on the interior element faces. Second, the HDG method has superconvergence properties that can be exploited to increase the convergence rate of the numerical solution by one order in some appropriate norms.[30,39,40] These advantages render the HDG method considerably more efficient than FDTD or FE methods for numerically solving Maxwell's equations. A detailed description of the HDG method is provided in the Supporting Information.

While the HDG method has been successfully applied to solve acoustic, elastic, and electromagnetic wave propagation problems more efficiently than other available FE techniques, this powerful method has not yet been widely adopted in the field of nanoplasmonics. The extreme size mismatch (~mm scale wavelength, ~100 μm scale loops, and ~nm scale gaps) present in our 3D device geometry can validate the ability of the HDG method to handle multiscale problems in the field of nanoplasmonics and THz optics.

DOI: 10.1021/ph500464j
ACS Photonics 2015, 2, 417−424

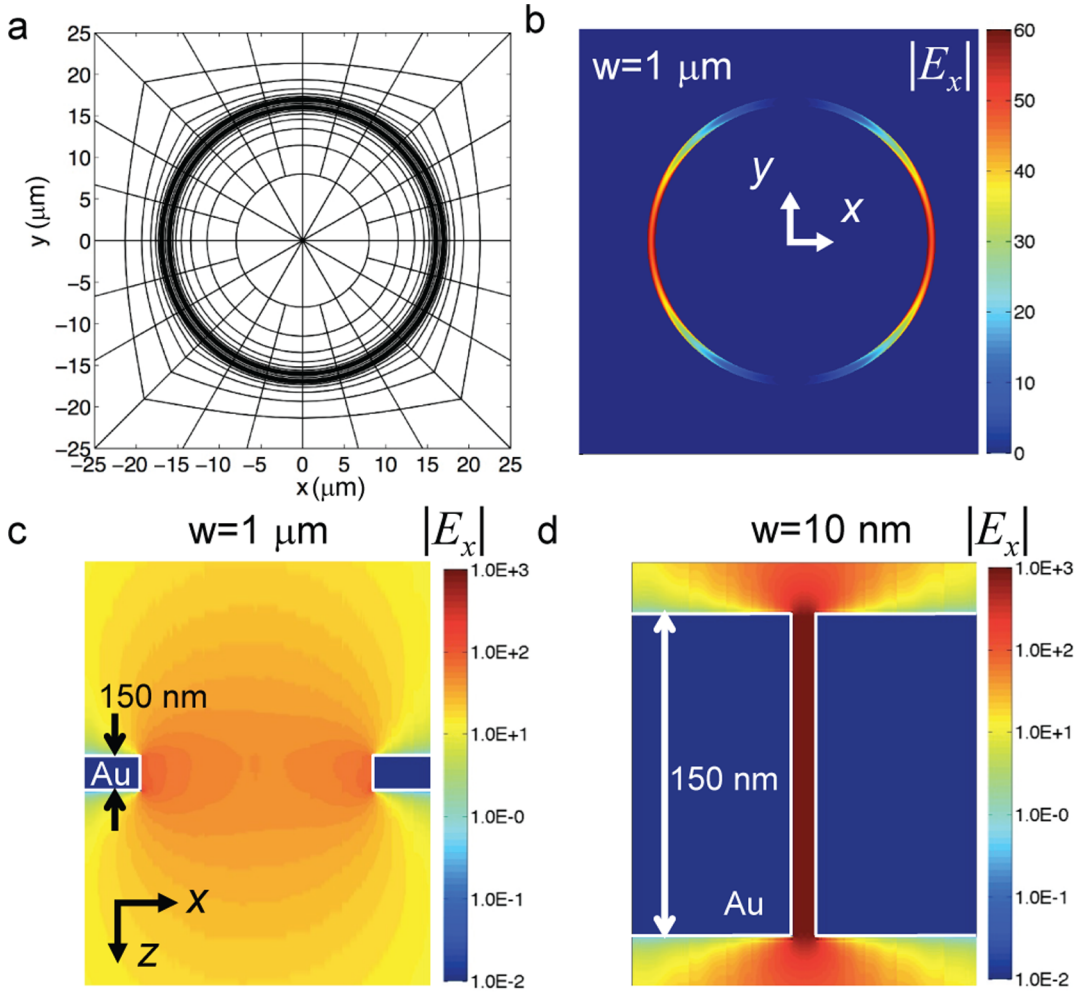

Figure 2. (a, b) Top-down views of (a) HDG meshes and (b) electric field ($|E_x|$) distribution in the annular gap of the gap size $w = 1$ μm at the resonance frequency of 1.95 THz with linear scale. (c, d) Cross-sectional view $|E_x|$ distributions for (c) the 1 μm gap at 1.95 THz and (d) the 10 nm gap at 0.625 THz with log-scale.

We use the HDG method to solve the time-harmonic Maxwell's equations on an anisotropic unstructured mesh of 22644 quartic hexagonal elements (Figure 2a). The accuracy of these results is verified by performing a grid convergence study in which we carry out the simulations on three consecutively refined meshes and observe that the difference in the field enhancement between the medium mesh and the fine mesh is less than 0.5% for the 10 nm gap and 0.1% for the 1 μm gap. Figure 2b shows the electric field amplitude ($|E_x|$) of the TE_{11} mode of an annular gap with a diameter of 32 μm and the width of a 1 μm, when the electric field polarization of the incident THz wave is along the x-axis. The resonance frequency (f_0) at this mode is determined by a cutoff frequency of $c/(ln_{\text{eff}})$, where c is speed of light, n_{eff} is the effective mode index, and l is the perimeter of the annular aperture.[12] Using the HDG method, the observed resonance frequencies (f_0) for the 1 μm gap and 10 nm gap are 1.95 and 0.625 THz, respectively. There are hot spots, or maximum field enhancements, at the gap regions perpendicular to the incident electric field polarization. In a cross-sectional view of the hot spot, we can compare the maximum field enhancements for both of the gaps, as shown in Figure 2c,d. Indeed, as the gap size shrinks from 1 μm to 10 nm, the maximum field enhancement inside the gap dramatically increases from 50 to 900. The simulated field map around the 10 nm gap (Figure 2d) shows that the enhanced electric fields are tightly localized within ~10 nm, that is, similar to the gap width, from the entrance and exit sides, and are nearly constant along its entire thickness of 150 nm inside the gap.

To experimentally characterize the spectral response of annular nanogap arrays, we performed THz-TDS[41,42] covering the frequency range from 0.1 to 1.0 THz (Figure 3a; see Methods for more details on the THz-TDS setup) and measured time traces of THz pulses transmitted through samples (Figure 3b). Annular nanogap arrays with a 32 μm diameter and a 50 μm array periodicity were prepared with different gap sizes (w = 2, 5, and 10 nm) in a 150 nm thick gold film on a Pyrex glass substrate using atomic layer lithography[26,27] (see Methods for details). By taking a Fourier transform of the time-domain data, transmitted electric field amplitude spectra are obtained in the frequency domain, as shown in Figure 3c. Each measured spectrum is normalized with respect to a reference signal passing through a bare glass substrate covered by a 3 mm × 3 mm stainless steel aperture. While the 2 nm gaps expose only 0.008% of the gold surface, the absolute transmission amplitude ($|E_x|$) of the input pulse measured through the sample was as high as 10% at the resonance frequency of 0.45 THz. Because direct THz transmission amplitude ($|E_x|$) measured through an unpatterned 150 nm gold film is below 0.1%, this extraordinary THz

DOI: 10.1021/ph500464j
ACS Photonics 2015, 2, 417−424

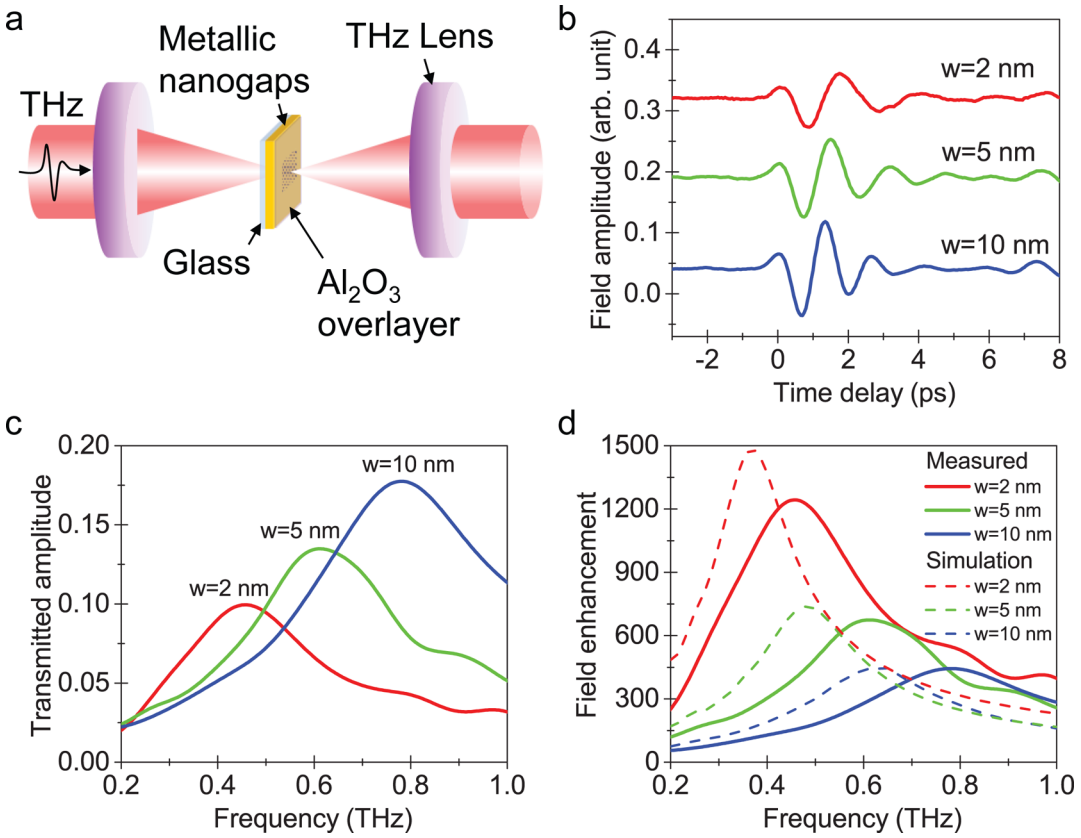

Figure 3. (a) Experimental setup of THz-TDS using Tsurupica lens to focus the THz waves on the annular nanogap sample. Normally incident THz waves illuminate the sample from the substrate side. (b) Transmitted electric field amplitudes ($|E_x|$) through the annular gaps of the gap sizes w = 2, 5, and 10 nm in the time-domain. (c) Fourier-transformed THz transmission amplitude ($|E_x|$) spectra, normalized by the reference signal through a bare substrate. (d) Electric field enhancement spectra in the same frequency domain as (c). Solid lines indicate measured field spectra, determined by THz-TDS. Dashed lines indicate numerically simulated field spectra, determined by the HDG method.

transmission is primarily due to the field enhancement in the annular gaps.

To infer field enhancement factors inside the gap from these measurements, we use Kirchhoff's diffraction formalism.[42] We normalized the transmission amplitude ($|E_x|$) spectra by each coverage ratio of the nanogaps and obtained the resulting field enhancement spectra in Figure 3d (solid lines), showing the increasing enhancement factor with the decreasing gap size. We also experimentally observed the maximum field ($|E_x|$) enhancement factor of 1250 from the 2 nm gap devices. This value is an average field enhancement factor on the whole gap area. Also, due to a large difference in refractive indices between metal and dielectric layer (air or substrate), the error in the field enhancement obtained using the perfect electric conductor approximation is less than 1%.[27]

Discrepancies that arise when comparing the experiments (Figure 3d, solid lines) and the HDG simulations (Figure 3d, dashed lines) can be attributed to the following facts. First, although in our simulation we used the thickness-dependent dielectric constants for the thin Al_2O_3 layers,[27,43] the effective refractive index of the Al_2O_3 film may be smaller than the reported thickness-dependent results due to voids or different deposition conditions. Second, in our simulation, the corners near the gap are assumed to be perfectly sharp, whereas in real device samples the corners are rounded, which effectively enlarges the gap size seen by the THz waves. The wider gap would reduce the field enhancement factor and also increase the resonance frequency. Finally, in our simulation, we used the dielectric functions of the metal obtained by Drude's formula with conventional bulk parameters for gold at THz frequencies.[44] However, those bulk parameters may not be accurate in describing optical properties of ultrathin metal films due to the surface scattering and grain boundary effects.[45] Especially, the damping constant in our device would not be as small as that in bulk metal,[45] wherein the enhancement factor could become smaller and the resonance frequency could also be blue-shifted. Despite these facts, we emphasize the good qualitative agreement between the simulations and the experiments, which demonstrates the tendency of the increasing field enhancement factor as the gap size is decreased.

Using the HDG method, we compare the sensitivities of the 1 μm gap and the 10 nm gap (same as the ones shown in Figure 2c,d) to thin dielectric overlayers. Compared with the 1 μm gap (Figure 4a), transmitted field enhancement spectra of the 10 nm gap presented in Figure 4b clearly show a red-shift in the peak position with adding the 10 nm thick Al_2O_3 overlayer in the simulations. Quantitatively, the normalized red-shift ($\Delta f/f_0$) of 1.6% for the 10 nm gap is over 3× larger than that of 0.49% for the 1 μm gap. These results predict that the nanogap array should possess higher sensitive to the change in local refractive index than micron-scale gap devices due to the stronger field confinement inside and near the nanogap.

To experimentally determine the sensitivity of our annular nanogap structures to dielectric thin films, we performed layer-by-layer sensing experiments using ALD. THz transmission spectrum is measured from a fixed location on each device before

DOI: 10.1021/ph500464j
ACS Photonics 2015, 2, 417−424

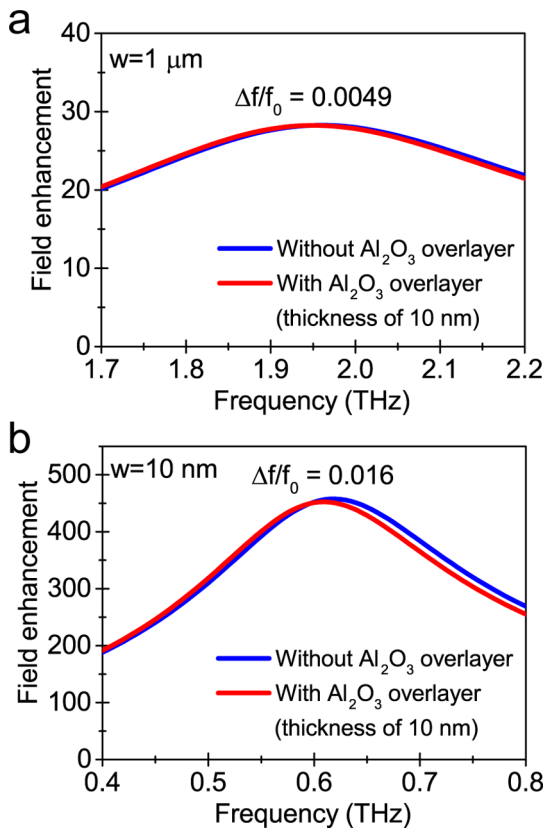

Figure 4. (a, b) Averaged field enhancement spectra of (a) the annular 1 μm wide gap and (b) the annular 10 nm wide gap, with (red lines) and without (blue lines) a 10 nm thick Al_2O_3 overlayer. All the data were numerically simulated by the HDG method.

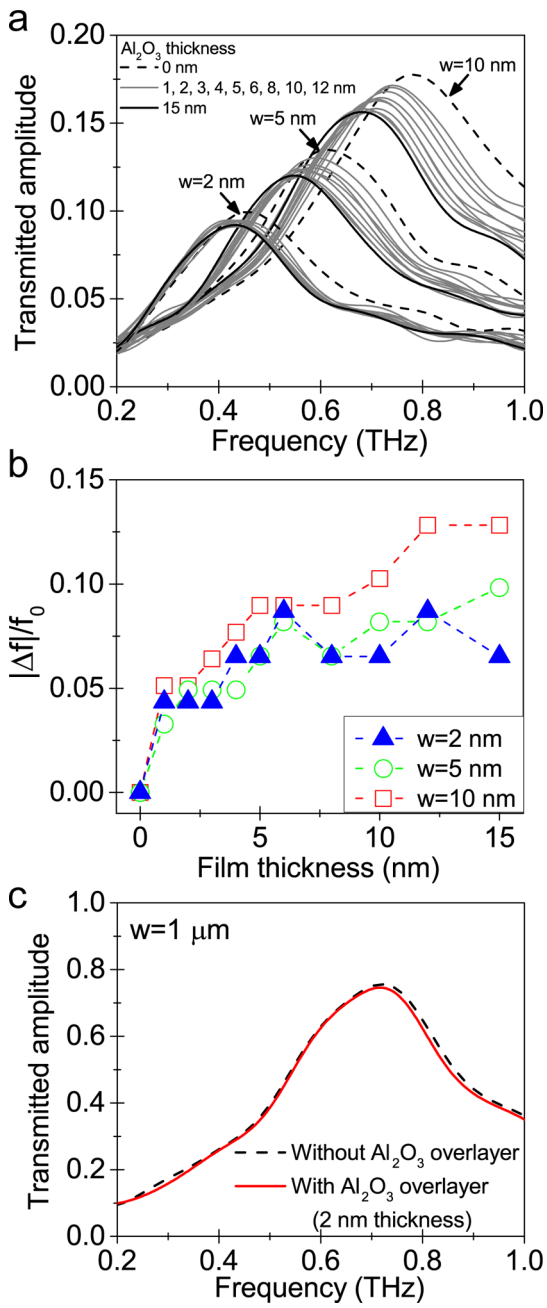

Figure 5. (a) Sequence of THz transmission amplitude ($|E_x|$) spectra through three types of annular gaps with w = 2, 5, and 10 nm as the thickness of the ALD-deposited Al_2O_3 overlayer increases from 0 to 15 nm. (b) Normalized spectral shift ($\Delta f/f_0$) of the resonance peak of the annular gaps with w = 2 (blue triangle), 5 (green circle), and 10 nm (red square). f_0 means each resonance frequency of the annular gaps without the Al_2O_3 overlayer. (c) Measured THz transmission amplitude ($|E_x|$) spectra through an array of annular gaps with a gap size of 1 μm, a diameter of 90 μm, and a period of 120 μm before (black dashed line) and after (solid red line) adding a 2 nm thick Al_2O_3 overlayer.

and after depositing 1 nm thick ALD-grown Al_2O_3 layer, and this process is repeated until the accumulated overlayer thickness reaches 15 nm. This method can precisely determine the spectral sensitivity as well as the probing range of various sensors and has been used to characterize plasmonic sensors in the visible range.[46−48] Figure 5a shows how the transmission amplitude ($|E_x|$) spectra of annular gap arrays change versus Al_2O_3 overlayer thicknesses. One can clearly observe red-shifts, that is, shifts toward longer wavelengths, in the resonance peak positions of the sub-10 nm gaps due to the Al_2O_3 overlayer that is as thin as 1 nm. The resonance frequency shifts are due to the increasing effective index n_{eff}, caused by the change of the local refractive index over the gaps when the material over the gaps is changed from air to Al_2O_3.[47,49] Figure 5b shows 3−5% red-shifts after adding a 1 nm thick Al_2O_3 overlayer onto the gaps, and the frequency shift gradually saturates to a maximum value after the thickness of the Al_2O_3 overlayer exceeds the gap size. This is because the evanescent field decays rapidly above the nanogap region and becomes less sensitive to refractive index changes with an increasing distance from the gap.[49,50] As expected, experimental results in Figure 5c show that annular apertures with a 1 μm gap width cannot detect the deposition of a 1 nm thick Al_2O_3 overlayer due to much weaker field confinement than sub-10 nm gaps.

Based on the field confinement effect only, one would expect that the thin-film detection sensitivity is higher for smaller gaps. However, measured spectral shifts due to a 1 nm thick Al_2O_3 overlayer are comparable for gap sizes of 2, 5, and 10 nm. To understand this result, we should consider the influence of the field decay length on the probing range as well as the effective mode index inside nanogaps. In fact, the device with 10 nm gaps shows larger spectral shift for the 15 nm thick Al_2O_3 overlayer because of its weaker field confinement than the devices with narrower gaps (2 and 5 nm), and increases the vertical probing range. As with other nanoplasmonic sensors, tighter confinement of THz waves in our structure increases the surface sensitivity, but this is achieved at the expense of the probing range. In

DOI: 10.1021/ph500464j
ACS Photonics 2015, 2, 417−424

addition, because of gap-plasmon dispersion effect,[27] narrower gaps (2 and 5 nm gaps in this case) have higher effective mode indices than the 10 nm gap. The higher effective mode index counteracts the spectral shift due to adding the Al_2O_3 overlayer outside the gap. This mechanism suggests that even higher sensitivity can be achieved by inserting materials inside the nanogap, if a scheme can be developed to completely remove the alumina film inside the gap and backfill the gap with target materials.

Due to practical limitations, the minimum ALD thickness in each step of our layer-by-layer sensing experiments was fixed at 1 nm. However, we can estimate the limit of detection for Al_2O_3 films using our system. For our 10 nm gap device, the spectral shift after adding the first 1 nm thick Al_2O_3 overlayer was 0.04 THz. Because the spectral resolution of our THz-TDS system is about 0.01 THz, we can estimate the minimum detectable thickness of ALD Al_2O_3 overlayer to be 0.25 nm. This result indicates that, in principle, even subnanometer-resolution detection of dielectric films may be possible using millimeter waves squeezed inside nanogaps.

CONCLUSIONS

We have experimentally demonstrated the detection of 1 nm thick dielectric overlayers using tightly confined THz waves. The results were also analyzed using the full 3D simulations performed by the HDG method, demonstrating its capability to handle challenging multiscale computational problems in nanoplasmonics and THz nanophotonics. Extreme squeezing of THz waves through sub-10 nm gaps enables sensing 1 nm thick Al_2O_3 overlayer with as much as 5% shift in the peak position. The intrinsic detection limit obtained from our measurements indicates that it should be possible to detect even sub-1 nm dielectric overlayers. Besides refractive index sensing, our THz nanogap platform can also be utilized to study surface-enhanced terahertz absorption.[20,51] In particular, our annular nanogap opens a new avenue to exploit atomically thin materials such as graphene and MoS_2,[52] detect monolayers of biomolecules, and investigate quantum tunneling[53] in the THz regime.

METHODS

Nanogap Fabrication via Atomic Layer Lithography. The nanogap is fabricated using the atomic layer lithography method developed in our previous work.[27] First, an array of circular holes with a diameter of 32 μm is fabricated in a gold film on a Pyrex glass substrate using negative resist (NR71−1500P) and photolithography, followed by metal deposition (150 nm Au with 3 nm Ti adhesion layer) via electron-beam evaporation and lift-off in a solvent (1165 remover). After cleaning with acetone, methanol, and IPA and blow dry with N_2 gas, the patterned metal film is conformally coated with a thin Al_2O_3 layer by ALD at 250 °C (Cambridge NanoTech Inc., Savannah). Trimethylaluminum and H_2O vapor were sequentially pulsed through the chamber and N_2 gas was used to purge the chamber after each injection. The thickness of the Al_2O_3 film was calibrated using ellipsometry on a control Si water placed in the same chamber, and the measured deposition rate for Al_2O_3 was 1.1 Å/cycle. After ALD, the trenches are filled with second metal by directional metal evaporation (Temescal). The metal deposited outside of the trench is easily removed using adhesive tape (single-sided 3M Scotch Magic Tape) without leaving any residue. To avoid deterioration of the nanogap at high temperature, we used low temperature (50 °C) ALD with a long nitrogen purge time to deposit Al_2O_3 overlayer on top of the nanogap, with a typical deposition rate of 1 Å per cycle.

Terahertz Time-Domain Spectroscopy. A terahertz pulse with a few picoseconds pulse width is generated from a GaAs-based photoconductive antenna (Tera-SED, Gigaoptics, GmbH) illuminated by a femtosecond Ti:sapphire laser pulse train with a center wavelength of 780 nm, 80 MHz repetition rate, and 90 fs pulse width (Mai Tai XF, Newport Corporation). As shown in Figure 3a, the *p*-polarized terahertz light was normally illuminated from the substrate side of the nanogap sample and the transmitted THz pulses through the samples are detected by electro-optic sampling method using a 1 mm thick ZnTe crystal (INGCRYS Laser System Ltd.).

ASSOCIATED CONTENT

Supporting Information

Hybridizable discontinuous Galerkin method. This material is available free of charge via the Internet at http://pubs.acs.org.

AUTHOR INFORMATION

Corresponding Authors

*E-mail: sang@umn.edu.

*E-mail: peraire@mit.edu.

Author Contributions

‡These authors contributed equally to this work (H.-R.P., X.C., and N.C.N.).

Notes

The authors declare no competing financial interest.

ACKNOWLEDGMENTS

This work was supported by the U.S. Department of Defense (DARPA Young Faculty Award N66001-11-1-4152; X.S.C., H.R.P., S.-H.O.) and the National Science Foundation (CAREER Award; S.-H.O.). J.P. and N.C.N. acknowledge support by the AFOSR (Grant Nos. FA9550-11-1-0141 and FA9550-12-0357) and the Singapore-MIT Alliance. Device fabrication was performed at the University of Minnesota, Nanofabrication Center, which receives support from the National Science Foundation (NSF) through the National Nanotechnology Infrastructure Network program, and the Characterization Facility, which has received capital equipment funding from NSF through the Materials Research Science and Engineering Center. S.-H.O. also acknowledges support from the Office of Naval Research Young Investigator Award. X.S.C. acknowledges support from the 3M Science and Technology Fellowship and the University of Minnesota Doctoral Dissertation Fellowship. The authors thank Fernando Reitich for helpful discussions.

REFERENCES

(1) Ebbesen, T. W.; Lezec, H. J.; Ghaemi, H. F.; Thio, T.; Wolff, P. A. Extraordinary optical transmission through sub-wavelength hole arrays. *Nature* **1998**, *391*, 667−669.

(2) Brolo, A. G.; Gordon, R.; Leathem, B.; Kavanagh, K. L. Surface plasmon sensor based on the enhanced light transmission through arrays of nanoholes in gold films. *Langmuir* **2004**, *20*, 4813−4815.

(3) Garcia-Vidal, F. J.; Martin-Moreno, L.; Ebbesen, T. W.; Kuipers, L. Light passing through subwavelength apertures. *Rev. Mod. Phys.* **2010**, *82*, 729−787.

(4) Luk'yanchuk, B.; Zheludev, N. I.; Maier, S. A.; Halas, N. J.; Nordlander, P.; Giessen, H.; Chong, C. T. The Fano resonance in plasmonic nanostructures and metamaterials. *Nat. Mater.* **2010**, *9*, 707−715.

DOI: 10.1021/ph500464j
ACS Photonics 2015, 2, 417−424

(5) Im, H.; Lee, S. H.; Wittenberg, N. J.; Johnson, T. W.; Lindquist, N. C.; Nagpal, P.; Norris, D. J.; Oh, S.-H. Template-stripped smooth Ag nanohole arrays with silica shells for surface plasmon resonance biosensing. *ACS Nano* **2011**, *5*, 6244−6253.
(6) Baida, F. I.; Van Labeke, D. Light transmission by subwavelength annular aperture arrays in metallic films. *Opt. Commun.* **2002**, *209*, 17−22.
(7) Poujet, Y.; Salvi, J.; Baida, F. I. 90% Extraordinary optical transmission in the visible range through annular aperture metallic arrays. *Opt. Lett.* **2007**, *32*, 2942−2944.
(8) de Waele, R.; Burgos, S. P.; Polman, A.; Atwater, H. A. Plasmon dispersion in coaxial waveguides from single-cavity optical transmission measurements. *Nano Lett.* **2009**, *9*, 2832−2837.
(9) Catrysse, P. B.; Fan, S. Understanding the dispersion of coaxial plasmonic structures through a connection with the planar metal-insulator-metal geometry. *Appl. Phys. Lett.* **2009**, *94*, 231111.
(10) Fan, W. J.; Zhang, S.; Minhas, B.; Malloy, K. J.; Brueck, S. R. J. Enhanced infrared transmission through subwavelength coaxial metallic arrays. *Phys. Rev. Lett.* **2005**, *94*, 033902.
(11) Williams, C. R.; Misra, M.; Andrews, S. R.; Maier, S. A.; Carretero-Palacios, S.; Rodrigo, S. G.; Garcia-Vidal, F. J.; Martin-Moreno, L. Dual band terahertz waveguiding on a planar metal surface patterned with annular holes. *Appl. Phys. Lett.* **2010**, *96*, 011101.
(12) Shu, J.; Qiu, C. Y.; Astley, V.; Nickel, D.; Mittleman, D. M.; Xu, Q. F. High-contrast terahertz modulator based on extraordinary transmission through a ring aperture. *Opt. Express* **2011**, *19*, 26666−26671.
(13) Maier, S. A. *Plasmonics - Fundamentals and Applications*, 1st ed.; Springer: New York, 2007; pp 89−104.
(14) O'Hara, J. F.; Singh, R.; Brener, I.; Smirnova, E.; Han, J. G.; Taylor, A. J.; Zhang, W. L. Thin-film sensing with planar terahertz metamaterials: sensitivity and limitations. *Opt. Express* **2008**, *16*, 1786−1795.
(15) Withayachumnankul, W.; Lin, H.; Serita, K.; Shah, C. M.; Sriram, S.; Bhaskaran, M.; Tonouchi, M.; Fumeaux, C.; Abbott, D. Sub-diffraction thin-film sensing with planar terahertz metamaterials. *Opt. Express* **2012**, *20*, 3345−3352.
(16) Ng, B. H.; Wu, J. F.; Hanham, S. M.; Fernandez-Dominguez, A. I.; Klein, N.; Liew, Y. F.; Breese, M. B. H.; Hong, M. H.; Maier, S. A. Spoof plasmon surfaces: A novel platform for THz sensing. *Adv. Opt. Mater.* **2013**, *1*, 543−548.
(17) Ng, B. H.; Hanham, S. M.; Wu, J.; Fernandez-Dominguez, A. I.; Klein, N.; Liew, Y. F.; Breese, M. B. H.; Hong, M. H.; Maier, S. A. Broadband terahertz sensing on spoof plasmon surfaces. *ACS Photon.* **2014**, *1*, 1059−1067.
(18) Gao, W.; Shu, J.; Reichel, K.; Nickel, D. V.; He, X.; Shi, G.; Vajtai, R.; Ajayan, P. M.; Kono, J.; Mittleman, D. M.; Xu, Q. High-contrast terahertz wave modulation by gated graphene enhanced by extraordinary transmission through ring apertures. *Nano Lett.* **2014**, *14*, 1242−1248.
(19) Brown, E. R.; Bjarnason, J. E.; Fedor, A. M.; Korter, T. M. On the strong and narrow absorption signature in lactose at 0.53 THz. *Appl. Phys. Lett.* **2007**, *90*, 061908.
(20) Park, H. R.; Ahn, K. J.; Han, S.; Bahk, Y. M.; Park, N.; Kim, D. S. Colossal absorption of molecules inside single terahertz nanoantennas. *Nano Lett.* **2013**, *13*, 1782−1786.
(21) Withayachumnankul, W.; O'Hara, J. F.; Cao, W.; Al-Naib, I.; Zhang, W. L. Limitation in thin-film sensing with transmission-mode terahertz time-domain spectroscopy. *Opt. Express* **2014**, *22*, 972−986.
(22) Nagel, M.; Bolivar, P. H.; Brucherseifer, M.; Kurz, H.; Bosserhoff, A.; Buttner, R. Integrated planar terahertz resonators for femtomolar sensitivity label-free detection of DNA hybridization. *Appl. Opt.* **2002**, *41*, 2074−2078.
(23) Zhang, J. Q.; Grischkowsky, D. Waveguide terahertz time-domain spectroscopy of nanometer water layers. *Opt. Lett.* **2004**, *29*, 1617−1619.
(24) O'Hara, J. F.; Withayachumnankul, W.; Al-Naib, I. A review on thin-film sensing with terahertz waves. *J. Infrared, Millimeter, Terahertz Waves* **2012**, *33*, 245−291.
(25) Homola, J. Surface plasmon resonance sensors for detection of chemical and biological species. *Chem. Rev.* **2008**, *108*, 462−493.
(26) Im, H.; Bantz, K. C.; Lindquist, N. C.; Haynes, C. L.; Oh, S.-H. Vertically oriented sub-10-nm plasmonic nanogap arrays. *Nano Lett.* **2010**, *10*, 2231−2236.
(27) Chen, X.; Park, H. R.; Pelton, M.; Piao, X.; Lindquist, N. C.; Im, H.; Kim, Y. J.; Ahn, J. S.; Ahn, K. J.; Park, N.; Kim, D. S.; Oh, S.-H. Atomic layer lithography of wafer-scale nanogap arrays for extreme confinement of electromagnetic waves. *Nat. Commun.* **2013**, *4*, 2361.
(28) Chen, X.; Park, H.-R.; Lindquist, N. C.; Shaver, J.; Pelton, M.; Oh, S.-H. Squeezing millimeter waves through a single, nanometer-wide, centimeter-long slit. *Sci. Rep.* **2014**, *4*, 6722.
(29) Solis, D. M.; Taboada, J. M.; Obelleiro, F.; Liz-Marzan, L. M.; Garcia de Abajo, F. J. Toward ultimate nanoplasmonics modeling. *ACS Nano* **2014**, *8*, 7559−7570.
(30) Nguyen, N. C.; Peraire, J.; Cockburn, B. Hybridizable discontinuous Galerkin methods for the time-harmonic Maxwell's equations. *J. Comput. Phys.* **2011**, *230*, 7151−7175.
(31) Hesthaven, J. S.; Warburton, T. Nodal high-order methods on unstructured grids - I. Time-domain solution of Maxwell's equations. *J. Comput. Phys.* **2002**, *181*, 186−221.
(32) Perugia, I.; Schötzau, D.; Monk, P. Stabilized interior penalty methods for the time-harmonic Maxwell equations. *Comput. Methods Appl. Mech. Eng.* **2002**, *191*, 4675−4697.
(33) Perugia, I.; Schotzau, D. The hp-local discontinuous Galerkin method for low-frequency time-harmonic Maxwell equations. *Math. Comput.* **2003**, *72*, 1179−1214.
(34) Hesthaven, J. S.; Warburton, T. High-order nodal discontinuous Galerkin methods for the Maxwell eigenvalue problem. *Philos. Trans. R. Soc., A* **2004**, *362*, 493−524.
(35) Busch, K.; Konig, M.; Niegemann, J. Discontinuous Galerkin methods in nanophotonics. *Laser Photonics Rev.* **2011**, *5*, 773−809.
(36) Cockburn, B.; Shu, C. W. Runge-Kutta discontinuous Galerkin methods for convection-dominated problems. *J. Sci. Comput.* **2001**, *16*, 173−261.
(37) Peraire, J.; Persson, P. O. The compact discontinuous Galerkin (CDG) method for elliptic problems. *Siam J. Sci. Comput.* **2008**, *30*, 1806−1824.
(38) Cockburn, B.; Gopalakrishnan, J.; Lazarov, R. Unified hybridization of discontinuous galerkin, mixed, and continuous Galerkin methods for second order elliptic problems. *Siam J. Numer. Anal.* **2009**, *47*, 1319−1365.
(39) Nguyen, N. C.; Peraire, J.; Cockburn, B. High-order implicit hybridizable discontinuous Galerkin methods for acoustics and elastodynamics. *J. Comput. Phys.* **2011**, *230*, 3695−3718.
(40) Nguyen, N. C.; Peraire, J. Hybridizable discontinuous Galerkin methods for partial differential equations in continuum mechanics. *J. Comput. Phys.* **2012**, *231*, 5955−5988.
(41) Grischkowsky, D.; Keiding, S.; Vanexter, M.; Fattinger, C. Far-infrared time-domain spectroscopy with terahertz beams of dielectrics and semiconductors. *J. Opt. Soc. Am. B* **1990**, *7*, 2006−2015.
(42) Seo, M. A.; Park, H. R.; Koo, S. M.; Park, D. J.; Kang, J. H.; Suwal, O. K.; Choi, S. S.; Planken, P. C. M.; Park, G. S.; Park, N. K.; Park, Q. H.; Kim, D. S. Terahertz field enhancement by a metallic nano slit operating beyond the skin-depth limit. *Nat. Photonics* **2009**, *3*, 152−156.
(43) Groner, M. D.; Elam, J. W.; Fabreguette, F. H.; George, S. M. Electrical characterization of thin Al_2O_3 films grown by atomic layer deposition on silicon and various metal substrates. *Thin Solid Films* **2002**, *413*, 186−197.
(44) Ordal, M. A.; Long, L. L.; Bell, R. J.; Bell, S. E.; Bell, R. R.; Alexander, R. W.; Ward, C. A. Optical-properties of the metals Al, Co, Cu, Au, Fe, Pb, Ni, Pd, Pt, Ag, Ti, and W in the infrared and far infrared. *Appl. Opt.* **1983**, *22*, 1099−1119.
(45) Liu, N.; Langguth, L.; Weiss, T.; Kastel, J.; Fleischhauer, M.; Pfau, T.; Giessen, H. Plasmonic analogue of electromagnetically induced transparency at the Drude damping limit. *Nat. Mater.* **2009**, *8*, 758−762.
(46) Whitney, A. V.; Elam, J. W.; Zou, S.; Zinovev, A. V.; Stair, P. C.; Schatz, G. C.; Van Duyne, R. P. Localized surface plasmon resonance

DOI: 10.1021/ph500464j
ACS Photonics 2015, 2, 417−424

nanosensor: A high-resolution distance-dependence study using atomic layer deposition. *J. Phys. Chem. B* **2005**, *109*, 20522−20528.
(47) Im, H.; Lindquist, N. C.; Lesuffleur, A.; Oh, S.-H. Atomic layer deposition of dielectric overlayers for enhancing the optical properties and chemical stability of plasmonic nanoholes. *ACS Nano* **2010**, *4*, 947−954.
(48) Lee, S. H.; Johnson, T. W.; Lindquist, N. C.; Im, H.; Norris, D. J.; Oh, S.-H. Linewidth-optimized extraordinary optical transmission in water with template-stripped metallic nanohole arrays. *Adv. Funct. Mater.* **2012**, *22*, 4439−4446.
(49) Park, H. R.; Koo, S. M.; Suwal, O. K.; Park, Y. M.; Kyoung, J. S.; Seo, M. A.; Choi, S. S.; Park, N. K.; Kim, D. S.; Ahn, K. J. Resonance behavior of single ultrathin slot antennas on finite dielectric substrates in terahertz regime. *Appl. Phys. Lett.* **2010**, *96*, 211109.
(50) Garcia-Vidal, F. J.; Moreno, E.; Porto, J. A.; Martin-Moreno, L. Transmission of light through a single rectangular hole. *Phys. Rev. Lett.* **2005**, *95*, 103901.
(51) Le, F.; Brandl, D. W.; Urzhumov, Y. A.; Wang, H.; Kundu, J.; Halas, N. J.; Aizpurua, J.; Nordlander, P. Metallic nanoparticle arrays: A common substrate for both surface-enhanced Raman scattering and surface-enhanced infrared absorption. *ACS Nano* **2008**, *2*, 707−718.
(52) Low, T.; Avouris, P. Graphene plasmonics for terahertz to mid-infrared applications. *ACS Nano* **2014**, *8*, 1086−1101.
(53) Esteban, R.; Borisov, A. G.; Nordlander, P.; Aizpurua, J. Bridging quantum and classical plasmonics with a quantum-corrected model. *Nat. Commun.* **2012**, *3*, 825.

DOI: 10.1021/ph500464j
ACS Photonics 2015, 2, 417−424